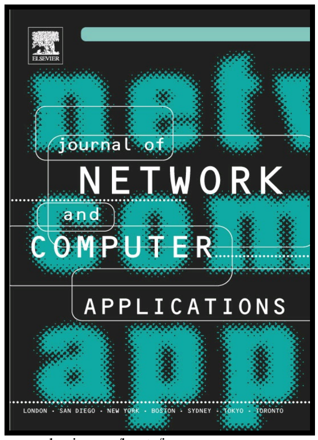

www.elsevier.com/locate/jnca

An Inferential Real-Time Falling Posture Reconstruction for Internet of Healthcare Things

Cong Zhang, Chin-Feng Lai, Ying-Hsun Lai, Zhen-Wei Wu, Han-Chieh Chao

PII: S1084-8045(17)30076-0
DOI: http://dx.doi.org/10.1016/j.jnca.2017.02.006
Reference: YJNCA1862

To appear in: *Journal of Network and Computer Applications*

Received date: 15 September 2016
Revised date: 3 January 2017
Accepted date: 18 February 2017

Cite this article as: Cong Zhang, Chin-Feng Lai, Ying-Hsun Lai, Zhen-Wei Wu and Han-Chieh Chao, An Inferential Real-Time Falling Posture Reconstructio for Internet of Healthcare Things, *Journal of Network and Compute Applications,* http://dx.doi.org/10.1016/j.jnca.2017.02.006

An Inferential Real-Time Falling Posture Reconstruction for Internet of Healthcare Things

Cong Zhang[a], Chin-Feng Lai[b], Ying-Hsun Lai[c], Zhen-Wei Wu[d], Han-Chieh Chao[a,*]

[a]*School of Mathmatic & Computer Science, Wuhan Polytechnic University, No. 1 Machi Rd., Dongxihu, Wuhan, Hubei, China*
[b]*Department of Engineering Science, National Cheng Kung University, No. 1 University Rd., Tainan, Taiwan*
[c]*Smart Network System Institute, Institute for Information Industry, No. 133, Sec. 4 Minsheng East Road, Taipei, Taiwan*
[d]*Department of Computer Science and Information Engineering, National Chung Cheng University, No. 168, University Rd.,ChiaYi, Taiwan*

Abstract

This study constructs a approach to reproduce the real-time falls of humans, which uses a triaxial accelerometer and triaxial gyroscope to detect the occurrence of a fall, and an attitude algorithm to estimate the angles of each part of the human body, where internet of healthcare things collects the information of each sensor, and a Bayesian Network deduces the next action. Inferential Bayesian probability could present more complete data of a fall to healthcare providers. Even if the data are damaged by the transmission network or equipment, the next action still could be deduced by Bayesian probability, and because the fall could be reproduced in a 3D Model on the client side, the fall occurrence is shown more intuitively, and could thus serve as reference for first aid.

Keywords: Posture Reconstruction, Sensors, Bayesian Network, Internet of Healthcare Things.

*Corresponding author
Email address: `hcc@niu.edu.tw` (Han-Chieh Chao)

1. Introduction

With the advance of internet of things, medicine has developed at a tremendous pace, and various medical technologies and equipment continue to progress. While the birth rate decreases year by year, the average life span of humans is prolonged, thus, the elderly population increases gradually; consequently, we usher in an aging society. The healthcare issues of the elderly have become increasingly urgent, and falls are the most common accidents of the elderly. A report [1-2] pointed out that, each year 13.7 % of the elderly fall, wherein, over a half fell twice or more. Many elderly people suffer injuries from a fall, followed by irremovability, unconsciousness, or a failure to save themselves. Moreover, as they wait for first aid, they have already lost the golden time for saving, thus, they may experience more severe injury or even indelible consequences. Therefore, it is an urgent issue to reduce the fall occurrences of the elderly. At present, most measures to detect falls focus on its occurrence, rather than reproducing the fall or reflecting the body part collided [3-4]. If these two drawbacks can be solved, the time spent to determine the reason for the fall and the injured body part can be reduced, thus, the elderly can be saved sooner. This paper contributes in the following three aspects:

(1) To detect the occurrence of a fall via triaxial accelerated velocities and angular accelerated velocities.

(2) To reproduce real-time human posture and falls.

(3) To deduce the probability of the next action.

2. Fall Detection and Posture Reconstruction

The major experimental methods employed in studies of fall detection could be classified into three categories: fixed type, non-fixed type, and mixed type, which has the strengths of the previous two types. Regarding the fixed fall detection method, a sensor is affixed in the environment, where a camera or other sensors are used to detect the occurrence of a fall [5-6]. As there is no need to carry or wear a sensor, it does not pose any burden to people; however, due to the limited recording angles, there are dead spaces, which is a big drawback in the detection of falls. Moreover, it has high cost and restricts the user to within a certain range. While the non-fixed fall detection method avoids the drawbacks of dead angles or limited space, the user must carry the sensor. To make the sensors more convenient for users, in addition to costing less than the first method, wearable devices are made as small as possible, and often include an accelerometer, gyroscope, and horizon finder. While the mixed type combines the strengths of the previous two methods, and greatly raises the recognition rate of falls, it also contains their shortcomings [7-8]. The analytical methods adopted by previous studies of the detection of falls were mainly the threshold analytical method and an intelligent algorithm.

2.1. Threshold Analytical Method and Relevant Studies

The analytical method is easiest. First, based on the data received by a sensor, a reference value is defined, which could be directly used to detect a fall. When the data received are lower or higher than the reference value, it could be determined that a fall has occurred. For instance, in the fall detection study of Bourke [8], the upper and lower thresholds were defined, as based on the steady signals of the daily actions (sit, lie down, and walk) of an acceleration sensor, where signals received within the thresholds implied daily actions, while those surpassing the thresholds implied a fall. In the experiment of his study, sensors were placed on the trunk and thigh to measure their recognition rate, and the results showed that when a sensor was placed on the trunk, its recognition rate was 100In the fall detection research of Dai [9], a smart phone containing a triaxial accelerator was used as a sensor, where the total acceleration and acceleration in the absolute vertical direction were combined, and the results under different circumstances were observed in order to define the fall threshold. This study compares Dai's system with products currently available on the market. Regarding the experimental method, this study places sensors on the chest, thigh, and waist in order to test the detection rates of sideways, forward, and backward falls, as well as daily actions, and the results show that the misjudgment rate of a sensor placed on the waist is the lowest. In the fall detection research of Sposaro and Tyson [10], a smart phone was used as a sensor, and the user could define the threshold according to his/her own situation. The smart phone must be placed on the chest or trunk in order to have the best detection result. When the device detected a signal higher than the threshold, it would send out an alarm. If the alarm was not turned off after a certain period of time, it was considered that the user could not move, and the system would contact pre-set emergency contacts via message and phone call. However, the system had limited recognition ability as it lacked a specific method to define its threshold. In addition, due to its lack of reference data, it was prone to misjudgment when the user was in another status, such as running or jumping. Although the advantage of the threshold analytical method was ease of implementation, the threshold definition would directly affect the recognition result rate of a fall, meaning if the threshold was not precise enough, it would lead to the misjudgment of a fall.

2.2. Intelligent Algorithm and Relevant Studies

Compared to the threshold analytical method, the intelligent algorithm is more complex, as it includes the calculation of posture simulation and has a higher fall detection rate. The data obtained via sensors are analyzed with specific methods to conclude the eigenvalue, and the learning features are used to establish a taxonomy module, which could classify the data obtained by the sensors. Common sorting algorithms include SVM, LDA, PCA, and ANN. In his study on fall detection and prevention [11], Delahoz explored the intelligent algorithm of fall detection and prevention, including the Decision Trees of the Machine Learning General Model, and compared Naive Bayes, K-Nearest Neighbor, and Support Vector Machines. In a fall detection study with an Android smart phone [12], Y. Shi adopted SVM and classified falls into five stages: normal, unstable, free fall, adjustment, and motionless. Recall was 90%, while precision was 95.7In his fall detection research [13], Sengto placed a triaxial accelerometer on the waist, and proposed the concept of the back propagation neural network (BPNN) to process the data of acceleration. He classified body postures including: falling activities, slow posture activities, and sudden posture activities. Recall was 96.25%, while specificity was 99.5Wu et al. [15] proposed a fall forecast and protection system, where human height was used to calculate the seconds between the fall and the collision, which would initiate the protection device. Zhang et al. [16] built a portable fall detection system, which broke through the space limit due to the reception of a computer; hence, users were protected outdoors. Compared with the threshold analytical method, the advantage of the intelligent algorithm was that the condition to determine the occurrence of a fall could be customized, and its accuracy was high. However, it was more complex and required a lot of data for study. Body postures were classified into various modules, and the learned data would determine the accuracy of fall detection. If body postures were not included in the learning modules, or if the intelligent algorithm did not consider such posture, misjudgment was prone to occur.

3. Inferential Real-Time Falling Posture Reconstruction

3.1. Fall Detection

This study used a triaxial accelerometer and gyroscope to sense the posture of each part of the human body, in order to simultaneously obtain triaxial accelerated velocities and triaxial angular accelerated velocities. Sensors are placed on five parts of the body, as shown in Figure 1. In order to obtain the real-time rotation angle of the five body parts, the figures of the triaxial accelerometer and gyroscope should be integrated. The detailed descriptions of the steps are, as follows.

3.1.1. Weighted Moving Average for Sensing Data

Upon initializing the End Device, this study required stable initial triaxial accelerated velocities and angular accelerated velocities, thus, we collected 200

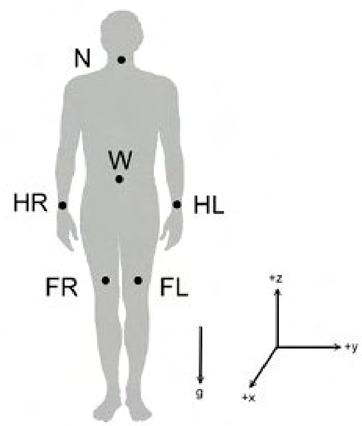

Figure 1: The parts of the human body with sensors.

samples to calculate the averages of the three-axis accelerated velocities (A_X, A_Y, and A_Z), and triaxial angular velocities (G_X, G_Y, and G_Z). First, A_X, A_Y, and A_Z are converted into the angles of the X-axis and Z-axis and Z-axis and Y-axis, via Eq.1 and Eq.2, respectively. In the human body coordinate system, only two angles are required to define the position of a body part. Thus, this study applies the formulas to obtain the angle of X-axis and the horizontal plane, and the angle of Z-axis and the vertical plane:

$$A_{cx} = \frac{tan^{-1}(\frac{A_z}{A_y}) \times 180}{\pi} \tag{1}$$

$$A_{cz} = \frac{tan^{-1}(\frac{A_x}{A_y}) \times 180}{\pi} \tag{2}$$

In order to render the triaxial accelerated velocities more accurate, and without noise interference, this paper uses weighted moving average to process the A_{cx} angle of the X-axis and the horizontal plane, as well as the A_{cz} angle of the Z-axis and the vertical plane. This study reserved n of the previous A_c A_{c1}, A_{c2}...A_{cn}, where A_{cn} was the final value. Each figure has a weight W W_1,

$W_2...W_n$, and their weighted average is $\overline{Ac}$, as shown in Eq.3.

$$\overline{Ac} = \frac{\sum_{i=1}^{n} W_i A_{ci}}{\sum_{i=1}^{n} W_i} \tag{3}$$

3.1.2. Kalman Filter for Sensing Data

The angular velocity obtained with a gyroscope had noise at all times, thus, when calculating angle, we must calculate angular velocity integration; though it was a small error, when accumulated over time, it would grow. The shorter the sampling time is, the bigger the error will be, thus, this paper required timely human angle data and long-term observation. Hence, high sampling frequency and long-term accumulation of data could lead to high angle drift and misjudgment of angle. Therefore, this paper adopts the Kalman filter and dynamic information of the target in order to remove the influence of noise and obtain a good estimated angle. First, this study calculates the integral of angular velocity G via Eq. 4, and via accumulation, obtains the current estimated angle; where t0 is the initial time, t1 is the current time, and G_0 is the initial angular velocity. Through integration, this study obtains current angle Ag.

$$A_g = \int_{t0}^{t1} (G - G_0)dt \tag{4}$$

Then, as an actual measured standard value S is required, this study reserved n previous $\overline{A_{c1}}$, $\overline{A_{c2}}$,..., $\overline{A_{cn}}$; where $\overline{A_{cn}}$ was the latest value, and they were divided by n to obtain the average with Eq. 5. The actual variance R is the result of the standard value minus $\overline{A_c}$ with Eq. 6. Then, the Kalman gain K could be calculated via Eq. 7. P is the deviation of the previous calculated value and the previous measured value; in this paper, the initial value of P is set as 1. To avoid the denominator of Eq. 7 being 0, 0.0025 was added to P, and P would be updated by each new K, as shown in Eq. 8. The K gain is used to calculate the final angle of Ag, as shown in Eq. 9. Through non-stop iteration, the angle gained by this study would become more accurate, and misjudgment would not occur due to noise.

$$S = \frac{\sum_{i=1}^{n} \overline{A_{ci}}}{n} \tag{5}$$

$$R = \frac{\sum_{i=1}^{n} (\overline{A_{ci}} - S)^2}{n-1} \tag{6}$$

$$K = \frac{P}{P+R} \tag{7}$$

$$P = (1-K) \times P \tag{8}$$

$$A_g = A_g + K(A_c - A_g) \tag{9}$$

3.1.3. Judgement of Fall

Upon obtaining the angles of the various parts of the human body, this study draws the current state of posture, and this visual model allows easy determination of the current posture state with the naked eye. However, as it is impossible for a user to monitor whether the person monitored is in danger, a fall detection system is required to remind the user. Common falls can occur due to loss of balance, and the body would produce accelerated velocity different from the normal state. At the moment of colliding with the ground or objects, a very large accelerated velocity, much higher than that of normal posture, would be produced. In fact, based on Figure 2, the scalar measurement of the accelerated velocity of a person falling while walking clearly shows that a very large scalar of accelerated velocity is generated in the red block. The change rates of both triaxial accelerated velocities and triaxial accelerated velocities would increase; Eq. 10 is used to calculate the scalar of triaxial accelerated velocities; Eq. 11 is used to calculate the change rate of triaxial accelerated velocities; where A_x, A_y, and A_z are the accelerated velocities in X-axis, Y-axis, and Z-axis.

$$A_{xyz} = \sqrt{{A_x}^2 + {A_y}^2 + {A_z}^2} \tag{10}$$

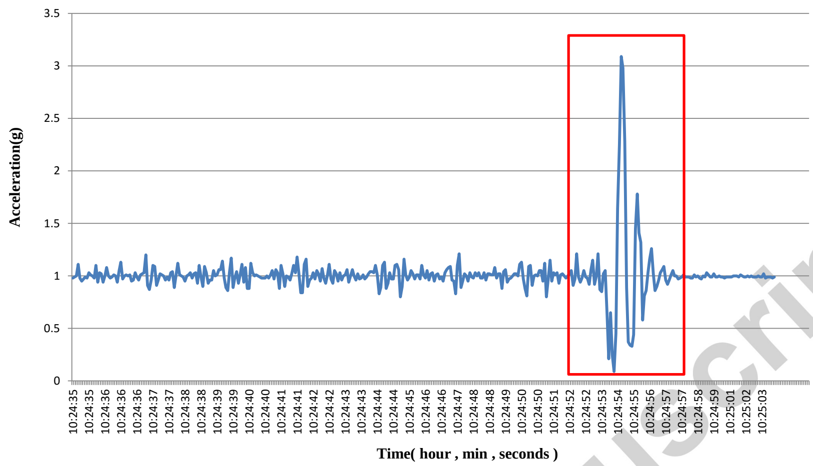

Figure 2: The scalar measurement of the accelerated velocity of a person falling.

$$A_v = \left| \frac{d(\sqrt{{A_x}^2(t) + {A_y}^2(t) + {A_z}^2(t)})}{dt} \right| \tag{11}$$

A_{xyz} and A_v are considered as the conditions to determine a fall. Moreover, according to the angles of inclination of the various body parts, we could detect the presence or absence of a fall, as shown in Figure 3. First, this study collects the sensor data of the various parts of the body, and calculates the angle of each part. When A_{xyz} and A_v were too large, this study temporarily considered that a fall had occurred; however, high accelerated velocity does not always imply the occurrence of a fall, as the user may be exercising, which produces high accelerated velocity, such as jumping or climbing stairs, and the user did not lose his/her balance. Hence, this study placed a sensor on the waist of a user to detect a fall, and classified a fall into four directions: forward, background, left, and right. If an angle was not within the four directions, the angles of the arms and legs would be used to determine falls in a sitting or lying position (Figure 4), and falls in the kneeling position (Figure 5). These two falls are not included in the four directions falls; hence, they should also be considered. If a fall does not fall into the above categories, the system would consider it as a jump or other posture and continue to detect. If a fall is directional, it would use the angle of the sensors on both hands to determine if the person used his/her hands for support while falling, or was supporting himself/herself with the elbow. Then, the posture of the legs is judged in a similar manner, meaning we would use the angle of the sensors on both legs to determine if the person is using his/her legs for support while falling, or is supporting himself/herself with their knees. After learning the direction and postures of the arms and legs, the final results are displayed to the user, and whether or not there was a fall is determined. As each fall is different, this study roughly classifies falls according to direction and the posture of arms and legs. Moreover, this study categorizes similar falls into one type in order to make it easier for healthcare providers or users to determine the direction of falls, support of hands, and bending of knees, and further analyze the injured part.

3.2. Inferential Real-Time Posture Reconstruction

This section constructs a human model and reproduces a fall. To visualize a fall requires a 3D model in line with a real human skeleton, where the angles of the five sensors (i.e. waist, right hand, left hand, right leg, and left leg) draw the real-time posture of a person. Then, a Bayesian Network is employed to deduce the next posture, in order to reduce the judgment range of the next posture and increase accuracy.

3.2.1. Category of Human Skeleton

The human skeleton shows that humans have many complicated bones, meaning it is impossible to design a specific device for each part. Thus, this study simplifies the skeleton, while maintaining precision, in order to establish a simple skeleton that does not affect the precision of the sensor data of posture

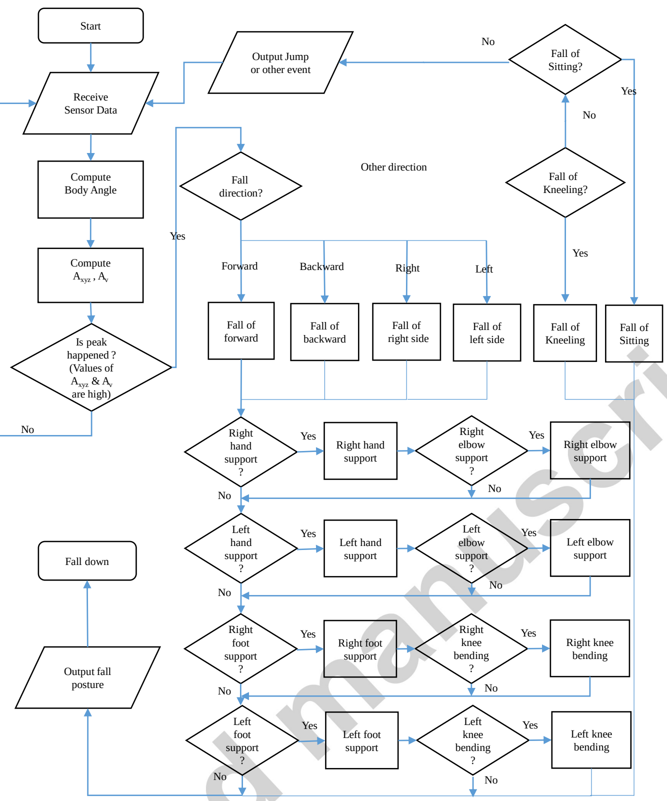

Figure 3: Diagram of fall detection.

reproduction in order to reproduce a fall. The degree of simulation lay in the quantity of sensors. This study considers the reproduction of most human body actions of the simplified human skeleton into 22 parts, as shown in Figure 6, including the Cranium, Cervical Vertebrae, Lumbar Vertebrae, Pelvic Girdle, Left Clavicle, Left Humerus, Left Ulna, Left Carpals, Left Finger, Left Femur, Left Tibia, Left Metatarsal, Left Toes, Right Clavicle, Right Humerus, Right Ulna, Right Carpals, Right Finger, Right Femur, Right Tibia, Right Metatarsal, and Right Toes.

Figure 4: Fall in a sitting or lying position.

Figure 5: Fall in the kneeling position.

3.2.2. Posture Structure of Human Skeleton

After establishing the human skeleton, this study defines the correlation between parent and child nodes, as shown by the arrows in Figure 7. When a parent node is in posture, so are its child nodes. For instance, the right thighbone moves with right shin bone, right metatarsal bone, and right toes; hence, we must define some rotating nodes. There are 14 rotating nodes, including the neck joint, waist joint, right clavicle joint, left clavicle joint, right elbow joint, left elbow joint, right wrist joint, left wrist joint, right hip joint, left hip joint, right knee joint, left knee joint, right ankle joint, and left ankle joint. Then, this study defines the bones influenced by each node. When a node is rotated,

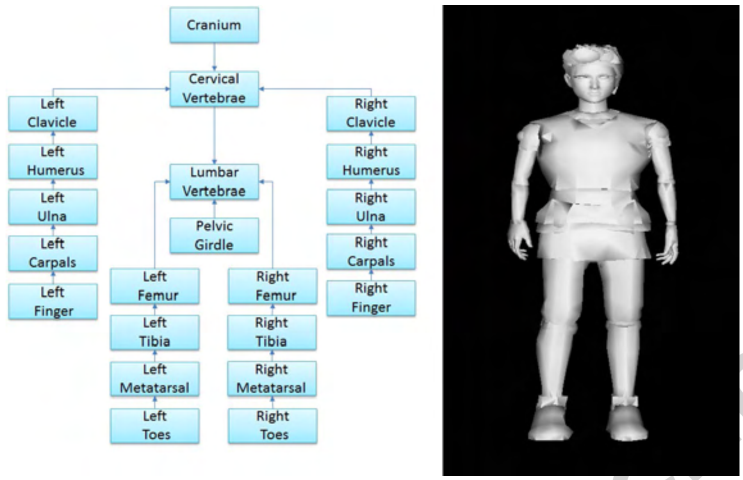

Figure 6: Reproduction of human skeleton.

its child nodes would move with it, followed by the movement of more child nodes. For instance, the right clavicle joint is moved with right clavicle and right humeri, while the right humeri is moved with right elbow joint, its child nodes, and the right ulna. The right wrist joint is moved with the right wrist and right fingers. After defining the correlation between bones, it is convenient to control each part without concern for the separation of bones. As the human body posture changes, the biaxial gyroscope can detect the movement and angular acceleration of object. The reason is the human limb does not swing and twisting actions occur simultaneously , So the features of three-axis acceleration and dual-axis gyroscope are enough to detect the changes of human postures.

3.2.3. Angle limit of skeleton

After establishing the 3D skeleton model and defining the correlation of nodes, this study defines the angle of each bone in order to restrict the rotation of each node and avoid impossible angles. Human joints could be roughly classified into three categories, uniaxial, biaxial, and multiaxial joints, as shown in Figure 8. The red areas refer to the range of rotation. When the rotation angle of each joint is restricted, it could avoid impossible angles, and determine joint limits. For instance, the X-axis angle of the right leg is $-90°$, and because the

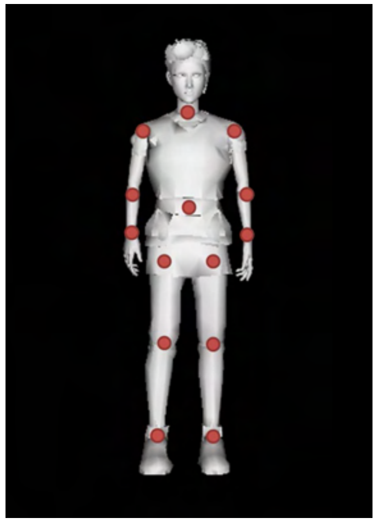

Figure 7: Correlation between parent and child nodes of the human body with sensors.

X-axis angle of the right hip joint cannot be $-90°$, it could be concluded that the rotated joint is the right knee.

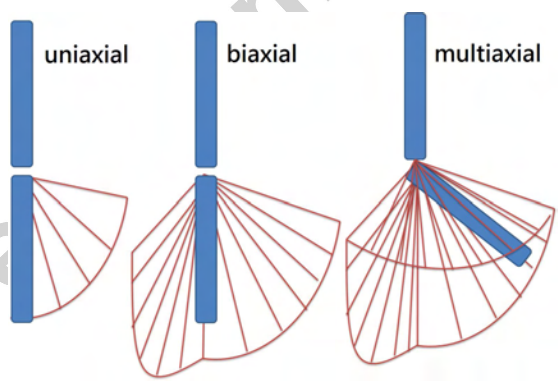

Figure 8: Three categories of joints.

3.2.4. Inference of Posture in a Bayesian Network

This section explains how to use a Bayesian Network to infer the next body posture, which serves as the reference angle of the next data. The probability table of a Bayesian Network could reduce the range of angles. When the next data appear, we could directly select an angle from the range, and infer whether the next figure would be within a reasonable range. If the next angle surpasses the deduced angle range, the angle would not be used, and the deduced angle would be kept. The following paragraphs explain the steps to establish a probability table for a Bayesian Network. First, this study uses a previous angle to infer the next angle with EMA, which uses the moving average of exponential diminishing weight, where the weight influence of each figure exponentially decreases with time, thus, more recent data has greater weight influence, while older figures have a certain weight. The degree of weight is determined by constant α, which is between 0 and 1. A user could adjust α in order to determine the degree of weight, as shown in Eq. 12. EMA_n refers to the estimated value of the next angle; while $EMAn-1$ refers to the estimated value of the previous angle, and EMA_{n-1} is the actual angle. As shown in Eq. 13, EMA_n is theoretically an infinite series. Because 1- is smaller than 1, the figures of each item would be smaller and smaller, and thus, could be ignored. The denominator would be close to $\frac{1}{\alpha}$.

$$EMA_n = EMA_{n-1} + \alpha(Ag_{n-1} - EMA_{n-1}) \tag{12}$$

$$EMA_n = \frac{Ag_{n-1} + (1-\alpha)Ag_{n-2} + (1-\alpha)^2 Ag_{n-3} + (1-\alpha)^3 Ag_{n-4} + \cdots}{1 + (1-\alpha) + (1-\alpha)^2 + (1-\alpha)^3 + \cdots} \tag{13}$$

When the inferred value of the next angle is obtained, proceed to build the Bayesian Network. First, define the directed and acyclic graphic, as shown in Figure 9. Where Ag is a previous actual angle; EMA_{n-1} is the previous inferred angle; and EMA_n is the current inferred angle, as calculated based on the EMA formula of the previous section. Thus, Ag and EMA_{n-1} are known. This study places five sensors on five body parts, and each part has two angles. The probability table of EMA_n is subject to the values of EMA_{n-1} and Ag; however, there was no need to define the entire table. For example, in order to establish the probability table of the angle of the waist sensor along the X-axis, $WA-A_{gx}$ and $WA-X-EMA_{n-1}$ are required to calculate EMA_n. The range of the probability table is based on the limitations of bones, and this study defines variable θ as the range of the probability limit of our inferred angles. When a fall or other accident occurs, the angles would change rapidly. As the sampling speed of our sensors is high, the difference among the measured angles would not be large. For instance, if the angle of a sensor is changed from 0° to 180° at the fasted speed possible, the angle data received by the user would not be changed directly from 0° to 180°. Instead, in line with the actual angle change of the sensor, the figure would change from 0°, to 10°, to 20°...and to 180°. Therefore, the difference between two angles would not be too large, and the change is gradual. Hence, this study defines variable θ as the threshold of the maximum angle change. Figure 10 shows the angle change from 0° to 90° and back to 0° at an extremely fast speed, which shows that most angle changes would not surpass 10°. Hence, this paper sets θ as 10°. During continuous monitoring of a human body, if the result of an upper angle minus a lower angle is greater than 10°, θ would be set as the angle. If any angle change is greater than θ, θ would be defined as the angle. Next, this study defines each probability in the probability table of EMA_n.

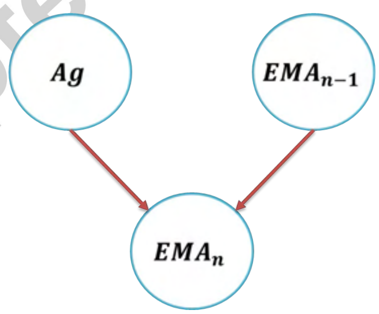

Figure 9: The directed and acyclic graphic of Bayesian Network.

First, this study sets inferred angle EMA_n to maximum, and the probability decreases as it becomes further apart from EMA_n. θ is considered as the range boundary of the probability, and the probability angle within θ was 0. The decreased probability is similar to the weighted moving average. First, the

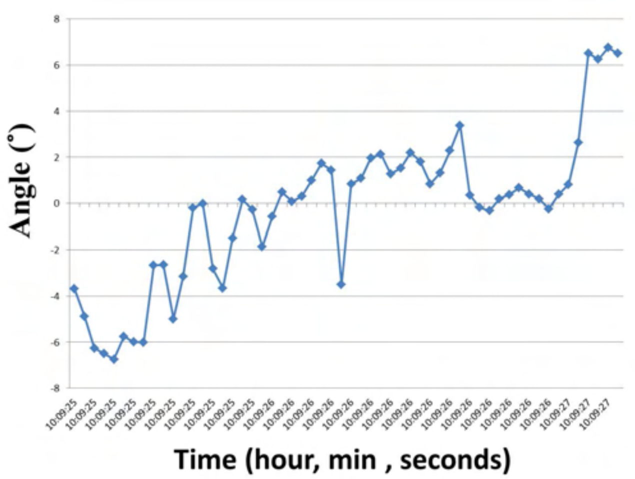

Figure 10: The angle change of human posture.

deviation figure Dev is calculated with Eq. 14, where EMA_n is the current inferred angle, Ag is the previous actual angle, and the actual angle is closest to the present.

$$Dev = |EMA_n - A_g| \tag{14}$$

The probability of EMA_n, $P(EMA_n)$, was shown in Eq.15. Within θ, the probability of other angles, $P(A_{ng})$, was shown in Eq.16. In Eq. 17, X is the absolute value of the result of the other angle minus the inferred angle. In other words, if it is different from EMA_n, its probability would also decrease. If the angles within θ surpassed the rotation limit of the joints, $P(A_{ng})$ would surpass θ, and should be set as 0. $P(A_{ng})$ is set as an impossible angle. The denominator of other $P(A_{ng})$ within θ must minus the total of numerators of those A_{ng} outside θ in order to comply with the principle of the Bayesian Network, meaning that the sum of probability of all the incidents is 1.

$$P(EMA_n) = \frac{Dev + \theta + 1}{(\theta + 1)^2 + (2\theta - Dev + 1)Dev} \tag{15}$$

$$P(A_{ng}) = \frac{(Dev + \theta + 1) - X}{(\theta + 1)^2 + (2\theta - Dev + 1)Dev} \tag{16}$$

$$X = |A_{ng} - EMA_n| \tag{17}$$

In the EMA_n angle probability table, N is the molecular of Eq.15; M is the denominator; and X is the absolute value of the difference between the other angle and the inferred angle. The probability table of the inferred angle of the other joint is completed in the same manner, and only the bone angle limit of each part is different. For example, starting from the latest actual angle, the blue area refers to the joint angle limit, while the green area refers to θ. Then, the probability of the inferred angle would be the biggest, and while it becomes further apart from the inferred angle, the probability would decrease to the two sides till the joint angle limit or θ limit. When Ag and EMA_{n-1} are entered, the probability table of the next inferred angle, EMA_n, is obtained. When the next actual angle is about to come, reduce the probability of the next angle. If the actual angle is outside the inferred angle range, consideration it as noise and discard it.

If the actual angle Ag_{n+1} is within the inferred angle range, Ag_{n+1} would replace EMA_n to update the probability table. When the same Ag and EMA_{n-1} appear in the next part, the probability table could be used as Ag, EMA_{n-1}, and inferred angle are the same. As the inferred angle is EMA_n, similar exponential changes would definitely occur. In other words, a similar angle change would appear with the previous actual angle for Ag. The next actual angle would be similar to the previous actual angle recorded. Thus, the probability table is used rather than the inferred EMA_n. With long-term monitoring of human angles, this study obtained many different angle probability tables corresponding to Ag and EMA_{n-1}, and used the actual angle to update the probability table, rendering our inferred angles more accurate.

4. Experimental Results

4.1. Experimental Environment

The systems used by this paper were Microsoft Windows 7 and Ubuntu 14.04. The CPU used was Intel(R) Core(TM) i5-4460@3.20GHz. The memory was 8.00GB. Angles were collected with Microsoft Windows 7. According to Ubuntu 14.04, this study was within the framework of IoTivity. The hardware devices used in this experiment paper are as shown in Figure 11.

This section probed into actual fall positions. According to different directions, this study classified falls into five types, forward, backward, left, right, and others. This system would reproduce most postures outside a fall. And the directions above were used as the classification basis of falls. Forward, backward, left, right, and other falls were the standard falls. This paper measured each type of fall 100 times, thus, there were 500 falls. For instance, there were 100 forward falls, and their postures were random. If the system correctly determined the direction and the posture of arms and legs, then the determination was correct; otherwise, it was wrong. The test results are as shown in Table 1.

Table 1: Falls Detection Results

Type	Test	Correct	Misjudgment	Correct Rate
Forward	100	98	0	98%
Backward	100	91	1	91%
Left	100	89	2	89%
Right	100	96	1	96%
Others	100	99	0	99%

4.2. Comparison between Kalman Filter and General Approach

This section compared the Kalman algorithm, as adopted in this paper, with the general gyroscope algorithm. First, we used the two algorithms in the situations of actual posture - Standing still and falling forward, backward, and sideways.

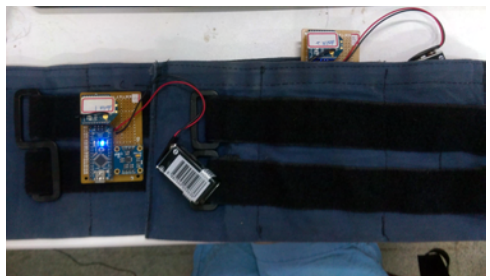

(a) Ankle

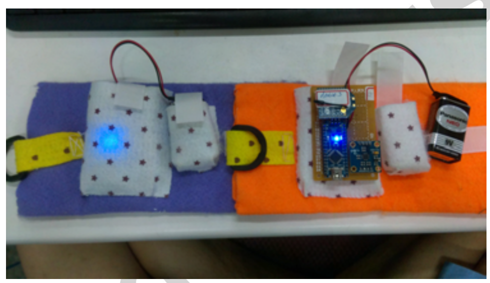

(b) Wrist

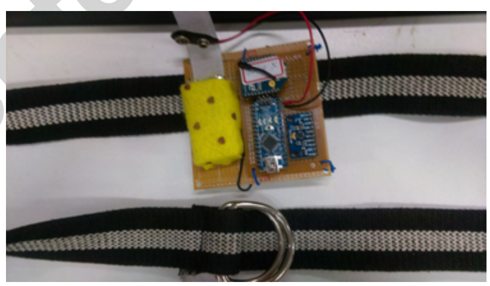

(c) Waist

Figure 11: Sensor Hardware Devices

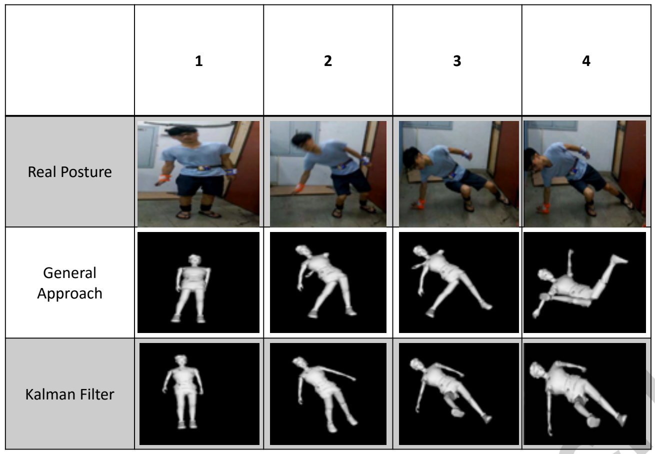

(a) Standing Still

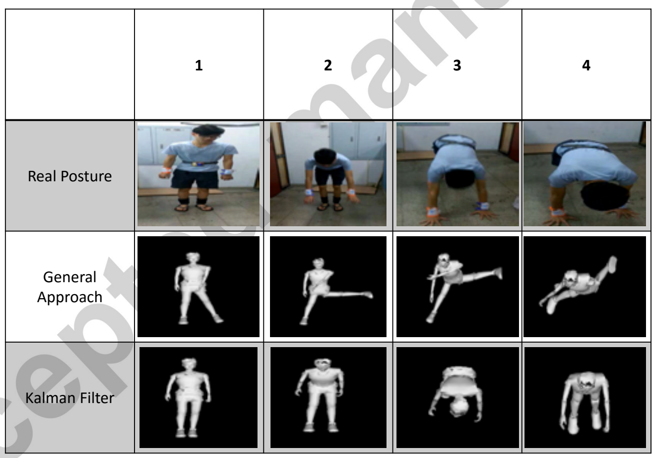

(b) Fall Forward

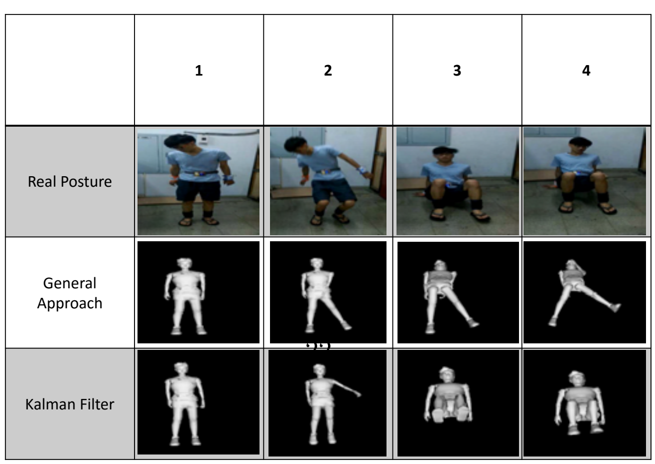

(c) Fall Backward

We compared the two algorithms in the situations of standing still (Figure 12(a)), fall forward (Figure 12(b)), fall backward (Figure 12(c)), and fall sideways (Figure 12(d)). Why did the general gyroscope algorithm have such big deviations? This study used actual data to compare the algorithm used in this paper and the general gyroscope integration algorithm. This study compared the angles along the X-axis of the sensor on the right hand. While the right hand remained still, the angle changes of the two algorithms were observed, and the results are as shown in Figure 13. Based on the test results, we can clearly see that the angle obtained with general gyroscope algorithm would gradually deviate from the actual angle with time; however, in fact, the angle of the sensor did not change much, and after 30 seconds, the deviation was greater than 0°. Next, the right hand repeatedly moved from 0° to −90° and back to 0°, and the results are as shown in Figure 14. Based on the test results, we can see that the angle obtained with general gyroscope algorithm was different from the actual angle. However, the angle obtained with the Kalman algorithm was closer to the actual angle. Next, the right hand repeatedly moved from 0° to −90° and back to 0°, and the results are as shown in Figure 15. Based on the test results, we can see that the angle changes obtained with general gyroscope algorithm were roughly correct; however, the deviation grew with time, while the angles obtained with the Kalman algorithm did not show cumulative error or loss of precision. Regarding the general gyroscope algorithm, the accumulated angular velocity was considered as the initial data. The angular velocity obtained with the gyroscope algorithm had noise. When we calculated the angle, we had to calculate the integral of the angular velocity, and though the error was small, the noise accumulated with time, resulting in bigger angle deviations. This paper adopted the Kalman Filter to omit noise and obtain a good estimated angle.

4.3. Comparison of the Inferred and Actual Angles

This section compared the inferred and actual angles. We compared the angles along the X-axis of the sensor on the right hand. The right hand repeatedly moved from 0° to −90° and back to 0°, and the results are as shown in Figure

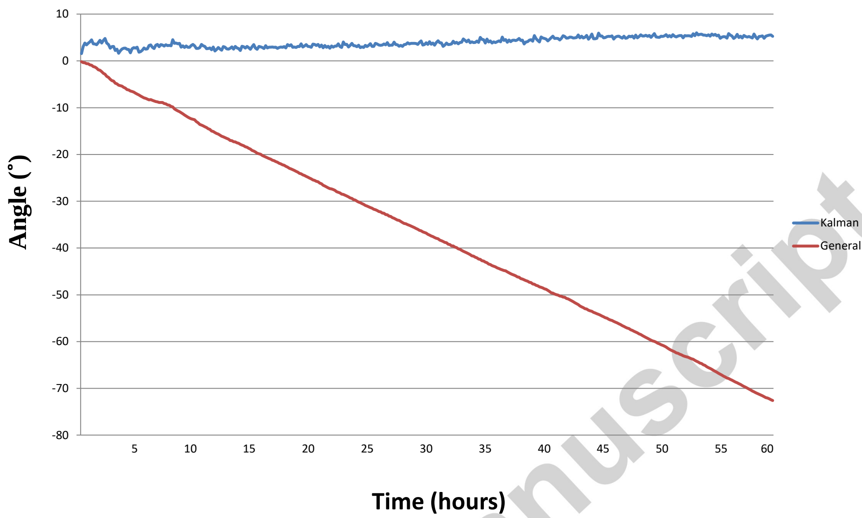

Figure 13: Angle changes of the two algorithms-case 1.

16. We can see that the error between the inferred and actual angles was not large, which implies that the practice of establishing the probability table of the Bayesian Network via the inferred angle in this paper is reliable. As mentioned in the previous section, when the actual and inferred angles were the same as previously, we would use the actual angle recorded previously to update the inferred angle. The right hand repeatedly moved from $0°$ to $-90°$ and back to $0°$, and the results are as shown in Figure 17. The green line refers to the improved inferred angle, which was closer to the actual angle. Certainly, only a small part of the probability table of the Bayesian Network was improved and replaced. When a user carries the device for a long time, the scope of the probability table of the Bayesian Network would expand, and more actual angles would replace the inferred angles, rendering the latter more accurate.

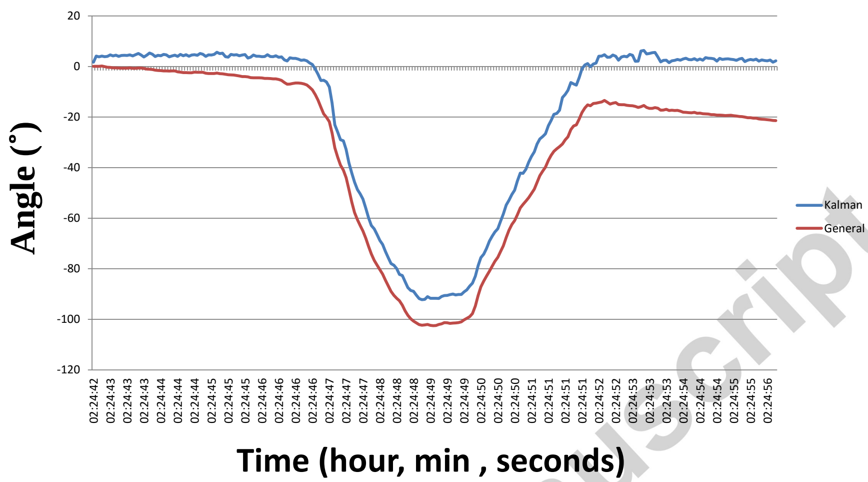

Figure 14: Angle changes of the two algorithms-case 2.

5. Conclusion

This paper offers a practical approach and model to reproduce body postures and falls in real-time, and calculates the angle of each part of the human body via triaxial accelerated velocities and a triaxial gyroscope. The attitude algorithm of this paper is not limited to the initial parts of a user, which greatly increases the convenience of use. Moreover, due to the transmission between internet of medical things, healthcare providers can monitor and observe the posture and fall of the user in the 3D model. The probability table of the Bayesian Network can provide healthcare providers with more complete fall data. Even more, it is easy to establish the proposed system in the real world due to the features of cheap hardware and light computing complexity.

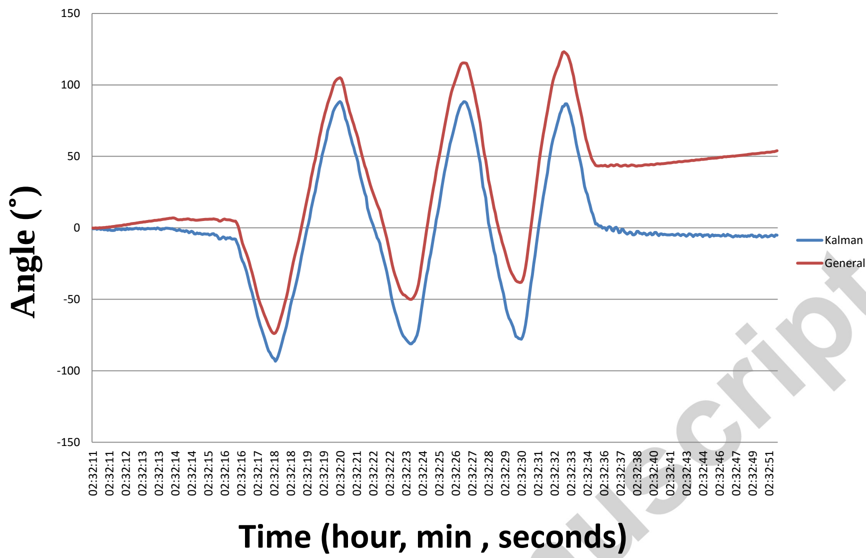

Figure 15: Angle changes of the two algorithms-case 3.

References

[1] T. Christine Cigolle et al., "The Epidemiologic Data on Falls, 1998-2010 More Older Americans Report Falling," JAMA Internal Medicine, Vol. 175, No.3, pp. 443-445, 2015.

[2] M. Kangas , R. Korpelainen , I. Vikman, L. Nyberg, T. Jms, "Sensitivity and False Alarm Rate of a Fall Sensor in Long-Term Fall Detection in the Elderly," Gerontology, Vol. 61, No. 1, pp. 6181, 2015.

[3] M. Stenhagen , H. Ekstrom , E. Nordell, S. Elmstahl, "Accidental falls, health-related quality of life and life satisfaction: a prospective study of the general elderly population," Arch Gerontol Geriatr, Vol. 58, No. 1, pp.95100, 2014.

[4] E. Tuunainen, J. Rasku, P. Jantti, I. Pyykko, "Risk factors of falls in

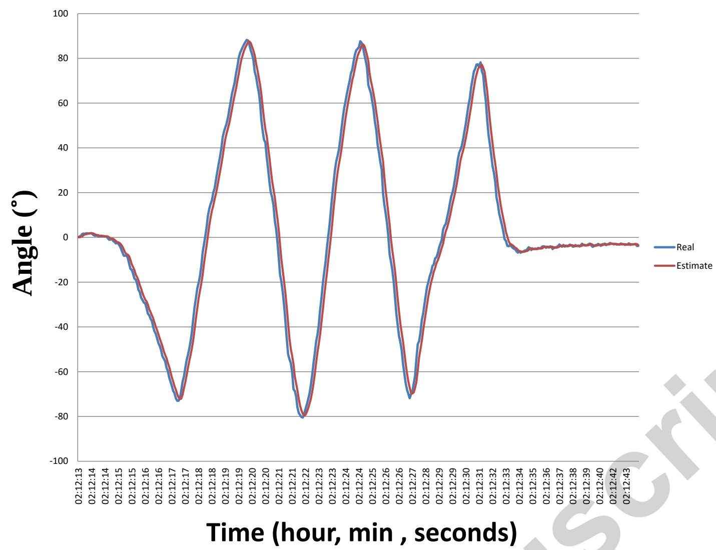

Figure 16: Comparison of the inferred and actual angles-case 1.

community dwelling active elderly," Auris Nasus Larynx, Vol. 41, No. 1, pp. 1016, 2014.

[5] F. Chiti, R. Fantacci, F. Archett, E. Messina, and D. Toscani, An Integrated Communications Framework for Context Aware Continuous Monitoring with Body Sensor Networks, IEEE JOURNAL ON SELECTED AREAS IN COMMUNICATIONS,Vol. 27, NO. 4, MAY 2009.

[6] H. Hawley-Hague , E. Boulton , A. Hall, K. Pfeiffer, C. Todd, "Older adults perceptions of technologies aimed at falls prevention, detection or monitoring: A systematic review," International Journal Medical Informatics, Vol. 83, No. 6, pp. 416426, 2014.

[7] M.T. Pham , A. Rajic , J.D. Greig, J.M. Sargeant, A. Papadopoulos, S.A. McEwen, "A scoping review of scoping reviews: advancing the approach and enhancing the consistency. Health expectations," International Journal of Public Participation in Health Care and Health Policy, Vol. 5, No. 4, pp. 371385, 2014.

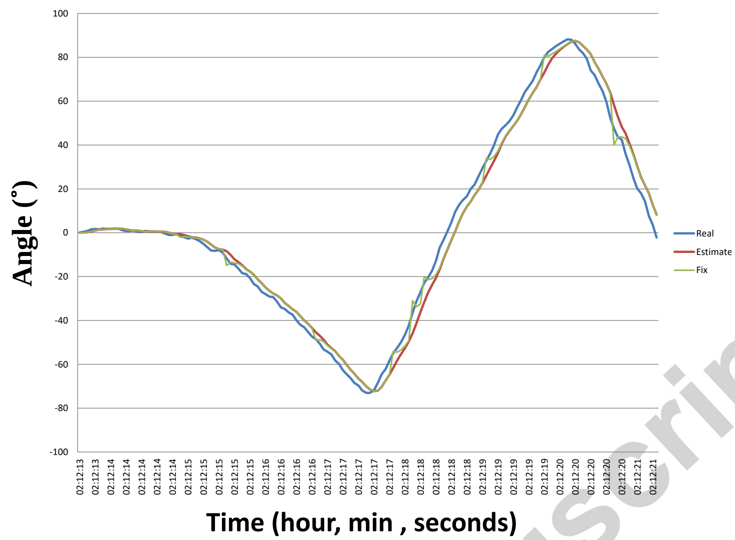

Figure 17: Comparison of the inferred and actual angles-case 2.

[8] A.K. Bourke, J.V. Obrien, G.M. Lyons, Evaluation of a threshold-based tri-axial accelerometer fall detection algorithm, Gait & posture, Vol. 26, No. 2, pp. 194-199, 2007.

[9] J. Dai, X. Bai, Z. Yang, Z. Shen, and D. Xuan, PerFallD: A Pervasive Fall Detection System Using Mobile Phones, Pervasive Computing and Communications Workshops (PERCOM Workshops), on Digital Object Identifier 8th IEEE International Conference, 2010.

[10] F. Sposaro and Gary Tyson, iFall: An Android Application for Fall Monitoring and Response, Annual International Conference of the IEEE Engineering in Medicine and Biology Society, 2009.

[11] Y. S. Delahoz,Survey on Fall Detection and Fall Prevention Using Wearable and External Sensors,Sensors 2014, 14, 19806-19842; doi:10.3390/s141019806, 2014.

[12] Y. Shi, Y.C. Shi, X. Wang,Fall Detection on Mobile Phones Using Features from a Five-Phase Model,9th International Conference on Ubiqui-

tous Intelligence and Computing and Autonomic and Trusted Computing, 47 September 2012, pp. 951956, 2012

[13] A. Sengto, T. Leauhatong, Human falling detection algorithm using back propagation neural network,5th Biomedical Engineering International Conference, 57 December 2012, pp. 15, 2012.

[14] Jui-Cheng Chiang Adaptive Collaborative Multi-Sensor Devices to Detect Body Position, Master's Thesis of Department of Engineering Sciences, National Cheng Kung University, 151 pp, 2009.

[15] G. Wu, S. Xue, Portable Preimpact Fall Detector With Inertial Sensors, IEEE Transactions on Neural Systems and Rehabilitation Engineering, Vol. 16, No. 2, pp. 178-183, 2008.